



ISTITUTO NAZIONALE DI RICERCA METROLOGICA Repository Istituzionale

Investigation of Ti/Au Transition-Edge Sensors for Single-Photon Detection

This is the author's accepted version of the contribution published as:

Original

Investigation of Ti/Au Transition-Edge Sensors for Single-Photon Detection / Xu, X.l., Rajteri, M., Li, J.j., Zhang, S., Pepe, C., Chen, J., Gao, H.f., Li, Q., Li, W., Li, X., Zhang, M.y., Ouyang, Y.y., Wang, X.s.. - In: JOURNAL OF LOW TEMPERATURE PHYSICS. - ISSN 0022-2291. - 209:3-4(2022), pp. 372-378. [10.1007/s10909-022-02818-5]

Availability:

This version is available at: 11696/76419 since: 2024-03-04T15:34:06Z

Publisher:

SPRINGER/PLENUM PUBLISHERS

Published

DOI:10.1007/s10909-022-02818-5

Terms of use:

This article is made available under terms and conditions as specified in the corresponding bibliographic description in the repository

Publisher copyright
SPRINGER NATURE

This version of the article has been accepted for publication, after peer review (when applicable) and is subject to Springer Nature's AM terms of use, but is not the Version of Record and does not reflect post-acceptance improvements, or any corrections.

(Article begins on next page)

1
2 **Investigation of Ti/Au Transition-Edge Sensors for**
3 **Single Photon Detection**
4

5 **Xiaolong Xu 1 • Mauro Rajteri 2 • Jinjin Li 1 • Shuo Zhang 3 •**
6 **Carlo Pepe 2,4 • Jian Chen 1 • Huifang Gao 1 • Qi Li 1 • Wei Li 1 •**
7 **Xu Li 1 • Mingyu Zhang 1 • Yanyan Ouyang 1 • Xueshen Wang 1**
8

9 *National Institute of Metrology (NIM), 100029 Beijing, China*

10 *Istituto Nazionale di Ricerca Metrologica (INRiM), 10135 Torino, Italy*

11 *ShanghaiTech University, 201210 Shanghai, China*

12 *Politecnico di Torino, 10129 Torino, Italy*
13
14

15 **Abstract** Transition-edge sensors (TES) are remarkable superconducting
16 devices for a wide range of radiation detection with the ability of both
17 energy resolution and counting photons. For the detection of single photons
18 at telecom wavelength, optical Ti/Au bilayer TESs are fabricated and
19 characterized. The superconducting transition temperature (T_c) of the Ti/Au
20 films are effectively tuned from 162 mK to 72 mK by increasing the relative
21 thickness ratio between the Au and Ti layer. The sensitive area is $20\ \mu\text{m} \times$
22 $20\ \mu\text{m}$, on which an $\text{SiO}_2/\text{SiN}_x$ antireflection structure is coated by an ICP-
23 PECVD process. The TES device shows an energy resolution of 0.19 eV and
24 can discriminate up to 36 incident photons, with an effective time constant
25 around 107 μs at 95 mK.
26

27 **Keywords** Superconducting transition-edge sensors • Ti/Au bilayer •
28 antireflection coating

29
30 **1 Introduction**
31

32 Superconducting transition-edge sensors (TESs) have been widely used for
33 single photon detection from near infrared, visible light, X-ray to even γ -ray.
34 The most distinctive feature of TESs is the single photon energy resolution
35 and the photon-number resolving (PNR) capability (when the photon energy
36 is already known) [1], but they also show high quantum efficiency [2],
37 negligible dark counts [3] and show great potential in quantum information
38 [4], dark matter detection [5], X-ray free-electron laser [6], satellite X-ray
39 observatory [7] and cosmic microwave background observatory [8]. In the

1 field of optical metrology, TESs will realize the quantum revolution of
2 photometry [9].

3 In this paper we report about the fabrication and preliminary
4 characterization of optical Ti/Au TESs for single photon detection at telecom
5 wavelength. The critical temperature T_c of Ti/Au superconducting films is
6 tuned by controlling the thickness ratio of the two layers. An antireflection
7 $\text{SiO}_2/\text{SiN}_x$ coating is deposited on the Ti/Au bilayer film before the
8 alignment of an optical fiber, and the simulated reflectivity is shown. The
9 TES device shows a high energy resolution (0.19 eV) and PNR capability up
10 to 36 photons.

11 2 TESs Fabrication

12 NIM fabricated TESs with two active areas ($10\ \mu\text{m} \times 10\ \mu\text{m}$ and $20\ \mu\text{m} \times 20\ \mu\text{m}$)
13 on the wafer. Considering the reliability of the optical fiber alignment
14 and to avoid optical geometric loss. In this paper we present preliminary
15 results for the TES with $20\ \mu\text{m} \times 20\ \mu\text{m}$ active area, which allows an easier
16 and better fiber optics alignment, but with a larger heat capacity that affects
17 the energy resolution. We have confirmed that the $20\ \mu\text{m} \times 20\ \mu\text{m}$ Ti/Au
18 TES has sufficiently ability to resolve 1550 nm single photon detection.

19 2.1 Ti/Au bilayer films

20 The Ti/Au bilayer films are deposited on double-polished 3-inch 500 μm
21 silicon substrates with 500 nm SiN_x layers on both sides using a magnetron
22 sputtering process. The base pressure is $\sim 10^{-6}$ Pa, and the sputtering pressure
23 is 0.1 Pa. Firstly, a 5 nm Ti film is sputtered as the adhesion layer. Then an
24 Au layer is deposited as the normal metal layer with a thickness d_{Au} of 60
25 nm. A variable thickness d_{Ti} of Ti layer (40 to 70 nm) is deposited on Au
26 layer.

27 **Tab. 1** The ρ_{eff} and R_q of Ti/Au films

Sample	Thickness/nm		$\rho_{\text{eff}}/\text{n}\Omega\cdot\text{m}$	R_q/nm
	Ti	Au		
NIM-21	70	60	76	1.11
NIM-22	60	60	65	1.02
NIM-23	50	60	57	1.04
NIM-24	40	60	53	1.01

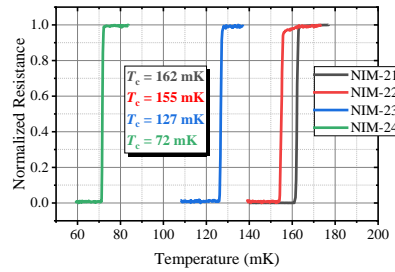
28 The effective resistivity ρ_{eff} , root mean square roughness R_q , and T_c of the
29 Ti/Au bilayer are measured for different $d_{\text{Ti}}/d_{\text{Au}}$ ratios. The ρ_{eff} is defined as
30 $R_{\square} \times (d_{\text{Au}} + d_{\text{Ti}})$, where R_{\square} is the sheet resistance. The ρ_{eff} is proportional to
31

32
33
34
35

Development of an Optical Ti/Au Transition-Edge Sensor for Single Photon Detection

1 the ratio $d_{\text{Ti}}/d_{\text{Au}}$ as shown in Tab.1. NIM-21 shows the highest $\rho_{\text{eff}} = 76$
 2 n Ω -m, and NIM-24 shows the lowest ρ_{eff} as 53 n Ω -m, which trends to the
 3 bulk Au resistivity ~ 22 n Ω -m [10]. The ρ_{eff} will be helpful for the resistance
 4 design of the TESs. The R_{q} are similar ~ 1 nm, indicating a good interface
 5 morphology between the Ti and Au layers. The smooth interface will make
 6 weak proximity effect [11,12].

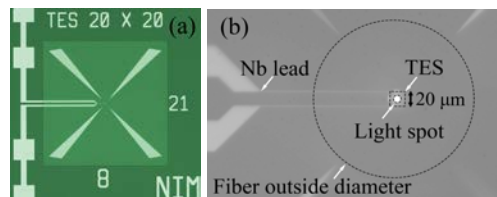
7 The T_{c} are measured in an adiabatic demagnetization refrigerator (ADR)
 8 system with a base temperature ~ 30 mK and are shown in Fig.1. The weak
 9 proximity effect occurs for the largest $d_{\text{Ti}}/d_{\text{Au}}$ ratio, and the T_{c} of NIM-21 is
 10 162 mK. Inversely, NIM-24 shows a stronger proximity effect which
 11 suppresses the T_{c} to 72 mK.
 12



13
 14 **Fig. 1** The T_{c} of the Ti/Au bilayers with different $d_{\text{Ti}}/d_{\text{Au}}$ ratios. (Color figure
 15 online)

16 2.2 Ti/Au TESs

17
 18 The optical image TES device is shown in Fig. 2. The $20 \mu\text{m} \times 20 \mu\text{m}$ active
 19 Ti/Au film area is defined by UV lithography followed by a lift-off process.
 20 The Nb superconducting leads for electrical wiring are also fabricated via a
 21 lift-off process. The thickness of the Nb layer should be thick enough to
 22 maintain its superconductivity after the following fabrication steps.
 23
 24

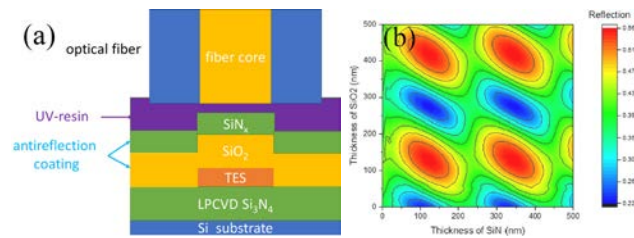


25
 26 **Fig. 2** Images of an optical Ti/Au TES with a $20 \mu\text{m} \times 20 \mu\text{m}$ sensitive area
 27 with Nb leads: (a) a whole view of the TES device; (b) the enlarged view of
 28 the device achieved during the optical fiber alignment process. A light spot
 29 can be observed at the center of TES to locate the position of optical fiber.
 30 (Color figure online)

1
2
3
4
5
6
7
8
9
10
11
12
13
14
15
16
17
18

2.3 Antireflection structure

An antireflection structure composed of SiO₂ and SiN_x dielectric layers is deposited on the TES devices to reduce the device reflectivity. The vertical stack structure is shown in Fig. 3(a). The SiO₂ and SiN_x layers are fabricated using an inductively coupled plasma assisted plasma-enhanced chemical vapor deposition (ICP-PECVD) method. The refractive index and extinction coefficient (n, k) are (1.47, 0), (1.92, 0), (4.03, 3.81), (0.56, 9.91) for SiO₂, SiN_x, Ti and Au at 1550 nm, respectively. These optical parameters were measured using a Horiba UVISSEL2 spectroscopic ellipsometers. The refractive index of the UV-resin for the fiber alignment process ($n = 1.56$) is similar to that of the fiber core ($n = 1.47$) [2]. With the above parameters, the reflectivity at 1550 nm is simulated and shown in Fig. 3(b). The lowest reflectivity is near 23%. The simulated transmittance is 10⁻³. To control the thickness accurately by the end point detection module of ICP-PECVD, 270 nm SiO₂ and 350 nm SiN_x are deposited on the TES device.



19
20
21
22
23
24
25
26
27
28
29
30
31
32
33
34
35
36

Fig. 3 (a) the cross section of the layer structure of the TES including the coupled optical fiber; (b) Simulation results of the reflectivity of the optical structure. (Color figure online)

2.4 Optical fiber alignment

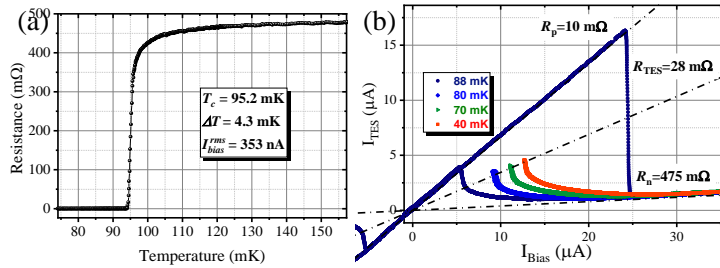
The optical fiber alignment process is operated with an inverted optical microscope with a near-infrared CCD. The TES device is fixed on the sample holder, and the optical fiber is aligned perpendicular to the device by a six-dimension adjustment frame. Fig.2b shows the backside image captured from the CCD. As the pig-tail optical fiber is connected to a 1550 nm light source, the fiber core emits a light spot. When the light spot locates at the center of the TES, the resin is cured with UV light to fix the fiber to the device.

3 TES characterization

Development of an Optical Ti/Au Transition-Edge Sensor for Single Photon Detection

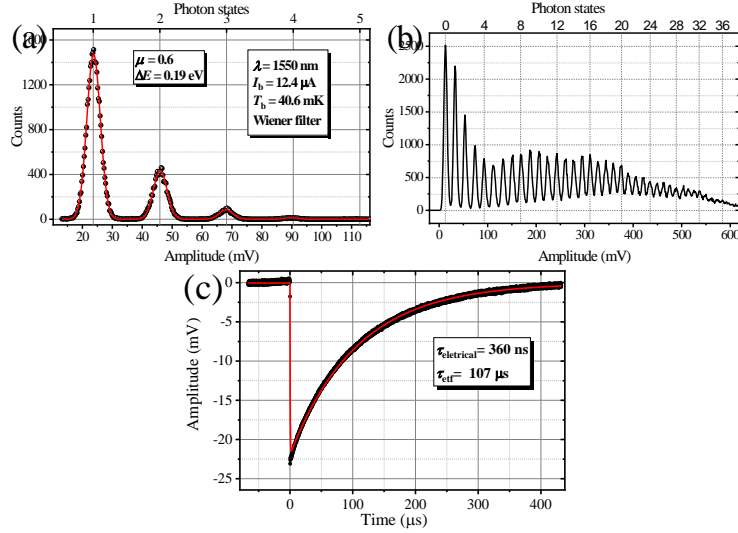
1 The NIM-23 device shows a T_c of 95.2 mK in the voltage-biased circuit with
 2 a DC-SQUID (Fig.4(a)). The TES's T_c in constant voltage mode shows
 3 around 30 mK shift compared with the film shown in Fig.1. The device
 4 shows a sharp superconducting transition with a width $\Delta T = 4.3$ mK. The
 5 TES working point is around 6% of R_n .

6 Fig. 4(b) shows the current flowing through TES I_{TES} as a function of
 7 I_{Bias} for the bath temperature T_b from 40 mK to 88 mK. The 20 m Ω shunt
 8 resistance R_s on the SQUID chip is selected. From the I_{TES} - I_{Bias} curves, the
 9 parasitic resistance $R_p = 10$ m Ω , the normal resistance of TES $R_n = 475$ m Ω
 10 and the working point resistance of TES $R_o = 28$ m Ω at 6% of R_n can be
 11 obtained. The heat capacity C of the Ti/Au bilayer is calculated as 2.2 fJ/K
 12 [13].
 13



14
 15 **Fig. 4** (a) The T_c of the TES device vs. temperature measured with a DC-
 16 SQUID (b) I_{TES} vs. I_{Bias} at different base temperatures. (Color figure online)

17
 18 The photon detection properties are characterized with a pulsed laser at
 19 1550 nm. With the statistics data of the pulse signals of photons detected by
 20 the TES device, the histograms of photo states are shown in Fig. 5(a) and
 21 Fig. 5(b). The energy resolution ΔE is defined as the full width at half
 22 maximum (FWHM) of the first photon state peak. Fig. 5(a) shows the count
 23 histogram for the pulses filtered with a Wiener filter [14]. The fit of the
 24 histogram with Gaussians convoluted with a Poissonian statistics (typical of
 25 lasers) gives a detected mean photon number $\mu = 0.6$ photons per pulse and
 26 an energy resolution $\Delta E = 0.19$ eV. In the same experimental conditions, we
 27 have also continuously reduced the attenuation of the laser during the
 28 acquisition, obtaining the histogram of Fig.5(b). In this case our TES can
 29 clearly distinguish up to 36 photons before reaching the saturation region.
 30 The typical averaged pulse response is shown in Fig. 5(c), which is fitted by
 31 a double exponential equation. The electrical time constant ($\tau_{electrical}$) is
 32 about 360 ns. And the response time constant (τ_{eff}) is about 107 μ s.
 33



1

2

3 **Fig. 5** Histograms of pulse height and photon states. The measurement
 4 conditions are reported in the insets. (a) The histogram is obtained from
 5 waveforms filtered with Wiener filter. The red curve is a fit with Gaussians
 6 convoluted with a Poissonian statistic; (b) The histogram is obtained directly
 7 with the signal acquired with a digital oscilloscope while the attenuation of
 8 the laser is reduced to show the whole photon states detectable with the TES;
 9 (c) Single photon pulse response. (Color figure online)

10

11 **4 Conclusions**

12

13 The optical Ti/Au bilayer TES device shows an energy resolution of 0.19 eV
 14 with a $20 \times 20 \mu\text{m}^2$ active area. The devices can discriminate up to 36
 15 photon states. The results have shown that TESs are promising detectors for
 16 counting single photon and promote the application of TES on the optical
 17 quantum metrology. In the future, the quantum efficiency will be evaluated
 18 and improved by optimal optical cavity.

19

20 **Acknowledgements**

21 This work was supported by Young Scientists Fund of the National Natural
 22 Science Foundation of China (Grant No. 61901432, 61701470), Science and
 23 technology project of State Administration for Market Regulation, China
 24 (2020MK153, 2019MK112) and the Fundamental Research Projects in
 25 Basic Scientific Research at NIM (AKYZD1903). INRiM authors would
 26 like to thank A. Barbone for the realization of the cryogenic experimental
 27 setup.

28

Development of an Optical Ti/Au Transition-Edge Sensor for Single Photon Detection

1 References

2

3 1. L. Lolli, E. Taralli, M. Rajteri, J. Low Temp. Phys. 167, 803 (2012) ,
4 DOI: 10.1007/s10909-012-0473-2

5 2. D. Fukuda et al., Opt. Express 19, 870 (2011) , DOI:
6 10.1364/OE.19.000870

7 3. A. J. Miller, S. W. Nam, J. M. Martinis, A. V. Sergienko, Appl. Phys.
8 Lett. 83, 791 (2003), DOI: 10.1063/1.1596723

9 4. R. H. Hadfield, Nat. Photonics 3, 696 (2009), DOI:
10 10.1038/nphoton.2009.230

11 5. F. Paolucci et al., J. Appl. Phys. 128, 194502 (2020), DOI:
12 10.1063/5.0021996

13 6. D. Li et al., J. Low Temp. Phys. 193, 1287 (2018), DOI: 10.1007/s10909-
14 018-2053-6

15 7. K. Nagayoshi et al., J. Low Temp. Phys. 199, 943 (2020), DOI:
16 10.1007/s10909-019-02282-8

17 8. J. R. Stevens et al., J. Low Temp. Phys. 199, 672 (2020), DOI:
18 10.1007/s10909-020-02375-9

19 9. J. C. Zwinkels, E. Ikonen, N. P. Fox, G. Ulm, and M. L. Rastello,
20 Metrologia 47, R15 (2010), DOI: 10.1088/0026-1394/47/5/R01

21 10. G. Kästle et al., Phys. Rev. B 70, 165414 (2004), DOI:
22 10.1103/PhysRevB.70.165414

23 11. K. Kengo et al., J. Low Temp. Phys. 193, 349 (2018), DOI:
24 10.1007/s10909-018-1995-z

25 12. X. Xu et al., Nanomaterials 11, 39 (2021), DOI: 10.3390/nano11010039

26 13. M. Rajteri et al., Metrologia 46, (2009), DOI: 10.1088/0026-
27 1394/46/4/S28

28 14. D. Alberto, et al., IEEE Trans. Appl. Supercond. 21, 285 (2011), DOI:
29 10.1109/TASC.2010.2087736

30